OPTICAL OBSERVATIONS AND ORBITAL PARAMETERS OF THE CLOSE DA PLUS dMe BINARIES BPM 71214, EUVE J0720−31.7, BPM 6502, AND EC 13471−1258

ADELA KAWKA,[1] STÉPHANE VENNES,[2] ROLF KOCH,[1] AND ANDREW WILLIAMS[3]

ABSTRACT

We have obtained photometric and spectroscopic observations of the close DA plus dMe binaries BPM 6502 and EC 13471−1258, and spectroscopic observations of the close binaries BPM 71214 and EUVE J0720−31.7. We have updated the ephemerides of BPM 6502 and EUVE J0720−31.7 with the spectroscopic measurements and obtained periods of 0.20162 and 0.15074 days for BPM 71214 and EC 13471−1258, respectively, by measuring the shift in Hα emission. Photometric variations in R and I due to reprocessing of incoming radiation from the hot white dwarf were observed in BPM 6502. We have also observed eclipses and ellipsoidal variations in B and R for EC 13471−1258, suggesting that the secondary is nearly filling its Roche lobe.

Key words: binaries: close — stars: individual (BPM 71214, EUVE J0720−31.7, BPM 6502, EC 13471−1258) — white dwarfs

1. INTRODUCTION

Post-common envelope (CE) binaries consist of a primary white dwarf and a late-type, low-mass, main-sequence secondary star in close orbit. These binaries are believed to have originated from wide binary systems, where the more massive star evolves off the main sequence and fills its Roche lobe, beginning mass transfer onto the less massive component, which can lead to the system being engulfed in a CE. Friction between the stellar components and the CE decreases the orbital separation and results in the expulsion of the CE. This mechanism is parametrized by the CE efficiency parameter (α_{CE}), and properties of the class of post-CE systems may help provide an empirical estimate to be compared with hydrodynamical calculations (see a discussion in O'Brien, Bond, & Sion 2001). Some of these close binaries further evolve to become cataclysmic variables.

High-dispersion spectroscopic observations and radial velocity studies of white dwarf stars help uncover new close binaries and determine their orbital parameters. Radial velocities are often determined from tracing Hα emission lines. The emission results from the reprocessing of EUV/FUV radiation in the hemisphere of the red dwarf illuminated by the white dwarf. This process has been observed in a number of stars showing photometric variations due to light reprocessing, such as the close binary systems PG 1224+309 (Orosz et al. 1999), GD 245 (Schmidt et al. 1995), CC Cet (Somers et al. 1996), and PG 1114+187 (Hillwig, Honeycutt, & Robertson 2000).

We have initiated a program of spectroscopic and photometric observations of known and suspected close binary systems involving white dwarf stars: BPM 6502, BPM 71214, EC 13471−1258, and EUVE J0720−31.7. Kawka et al. (2000, hereafter K2000) found the white dwarf BPM 6502 (LTT 3943) to be in close orbit with a red dwarf. They

measured an orbital period of 0.33678 ± 0.00003 days. BPM 71214 is a poorly studied binary, which has been classified as a post-CE system by Hillwig et al. (2000), and as a possible cataclysmic variable in hibernation or a precataclysmic variable by Livio & Shara (1987) with a period of 4 hr 20 minutes. Marsh (2000) quotes an orbital period of 0.202 days for this close binary and a period of 0.336 for BPM 6502. EC 13471−1258 has been observed as part of the Edinburgh-Cape Blue Object Survey, which observed the object as variable and classified it as a DA plus dMe eclipsing binary with an orbital period of 3 hr 37 minutes (Kilkenny et al. 1997). EUVE J0720−31.7 has been classified as a post-CE binary by Vennes & Thorstensen (1994) and has also been observed with the *Far Ultraviolet Spectroscopic Explorer* (*FUSE*) and the *Hubble Space Telescope* (*HST*) Goddard High Resolution Spectrograph (GHRS).

EUVE J0720−31.7 is a bright EUV/soft X-ray source (Dupuis, Vennes, & Bowyer 1997), and the emission originates from the hot photosphere of the young white dwarf. We note also that BPM 71214 has been observed with *ROSAT* as 1RXS J033243.5−085531 and was found to be an X-ray source with a count rate of 0.079 ± 0.02 counts s^{-1}, and EC 13471−1258 has also been observed an X-ray source with *ROSAT* as 1RXS J134951.0−131338 with a count rate of 0.14 ± 0.02 counts s^{-1} (Voges et al. 1999). The origin of the X-ray emission is uncertain but may involve an accretion disk, coronal activity, or simply thermal emission from a hot white dwarf atmosphere. However, the relative hardness of the emission in the last two objects would rather suggest the possibility of accretion onto the white dwarf or, more likely, of coronal activity.

We present new spectroscopic observations (§ 2.1) of BPM 6502, BPM 71214, EC 13471−1258, and EUVE J0720−31.7, and photometry (§ 2.2) in I and R for BPM 6502 and B and R for EC 13471−1258. We also examined archival *HST* Space Telescope Imaging Spectrograph (STIS) data (§ 2.3) of EC 13471−1258 to assist with a determination of the white dwarf parameters. We determine new orbital and stellar parameters (§ 3.1), and we examine the properties of the light curves searching for possible illumination effects or ellipsoidal variations (§ 3.2). We summarize in § 4.

[1] Division of Science and Engineering, Murdoch University, Perth, WA 6150, Australia; akawka@central.murdoch.edu.au, rkoch@central.murdoch.edu.au.

[2] Department of Mathematics, Australian National University, Canberra, ACT 0200, Australia; vennes@maths.anu.edu.au.

[3] Perth Observatory, Walnut Road, Bickley, Perth, WA 6076, Australia; andrew@physics.uwa.edu.au.
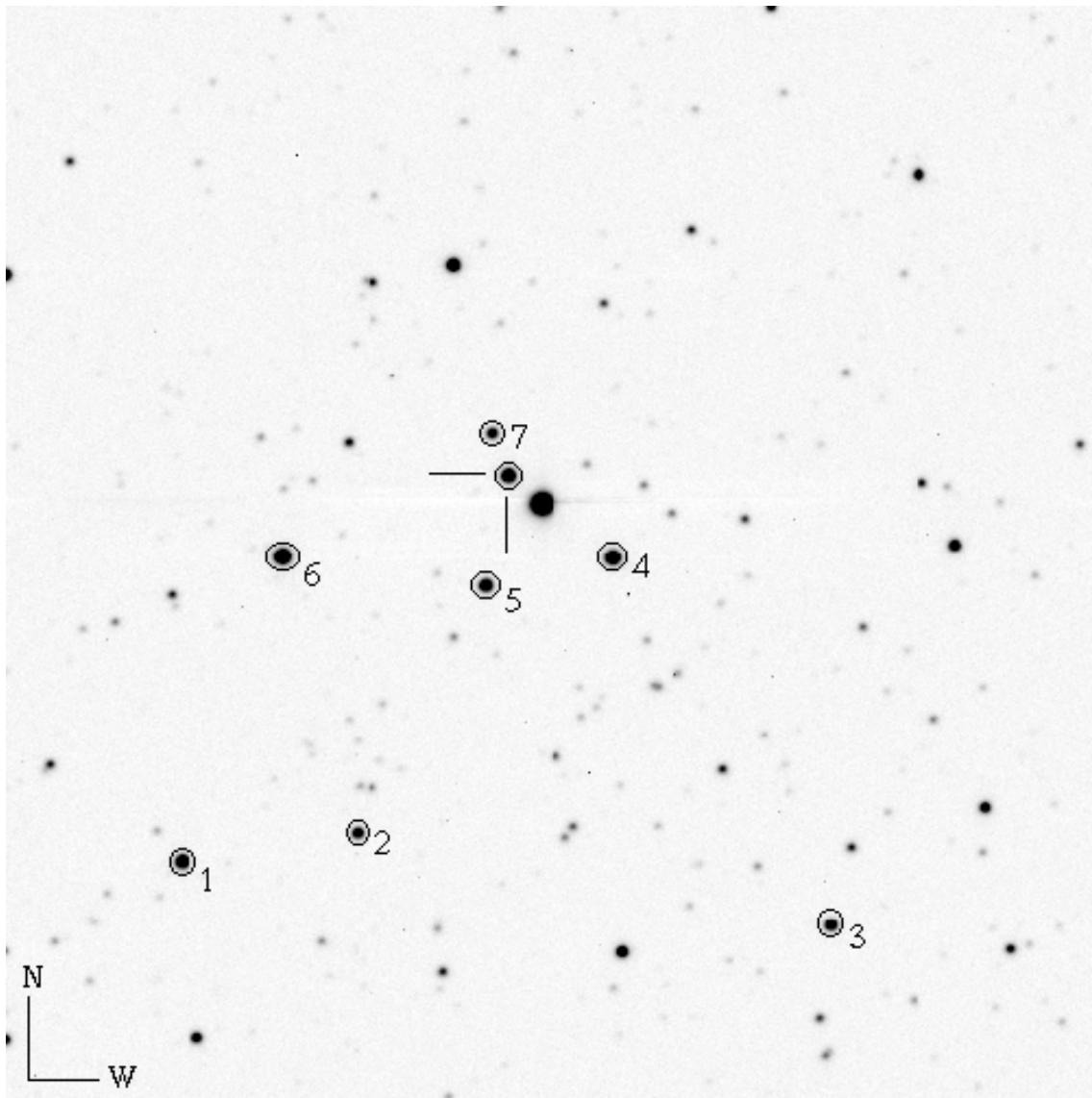
Fig. 1.—Image in R ($5' \times 5'$) showing BPM 6502 at the lines intersect and numbered reference stars used in the reduction of the images

2. OBSERVATIONS

Figures 1, 2, and 3 present finder charts for BPM 6502, BPM 71214, and EC 13471−1258. Vennes & Thorstensen (1994) present a chart for EUVE J0720−31.7.

2.1. Optical Spectroscopy

We observed the Hα line emission in the four binaries using the Cassegrain spectrograph attached to the 74 inch (1.9 m) telescope at Mount Stromlo Observatory (MSO) on 1999 October 10, November 10–15, 2000 February 4–9, March 1,31, 2002 January 26, 27, February 1, 11–14, March 1, 2, 5, 7–10, 30, 31, and April 1, 5–7, using the 1200 line mm^{-1} grating blazed at 7500 Å. We have used the 2K $\times$ 4K CCD camera binned 2 $\times$ 2. The spectra range from 6230 to 6830 Å, with a dispersion of 0.50 Å pixel^{-1}. A GG495 filter was used to cut out the second-order spectrum. The exposure times for the spectra were 30 minutes for BPM 6502, 10–15 minutes for BPM 71214, 15–20 minutes for EC 13471−1258, and 30–40 minutes for EUVE J0720−31.7 followed by an FeNe arc exposure of 5 s. We have also
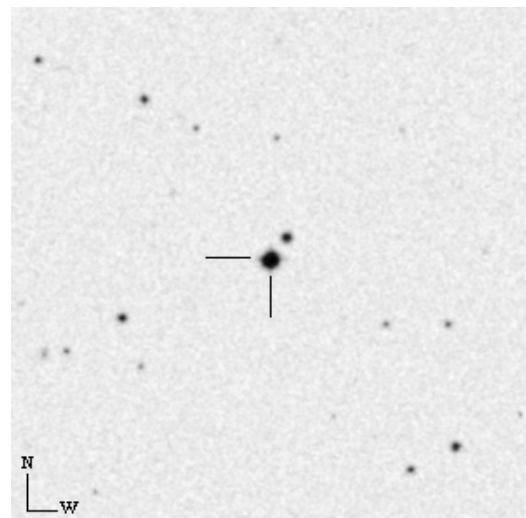

Fig. 2.—Second Generation DSS chart in R ($5' \times 5'$) indicating the position of BPM 71214.
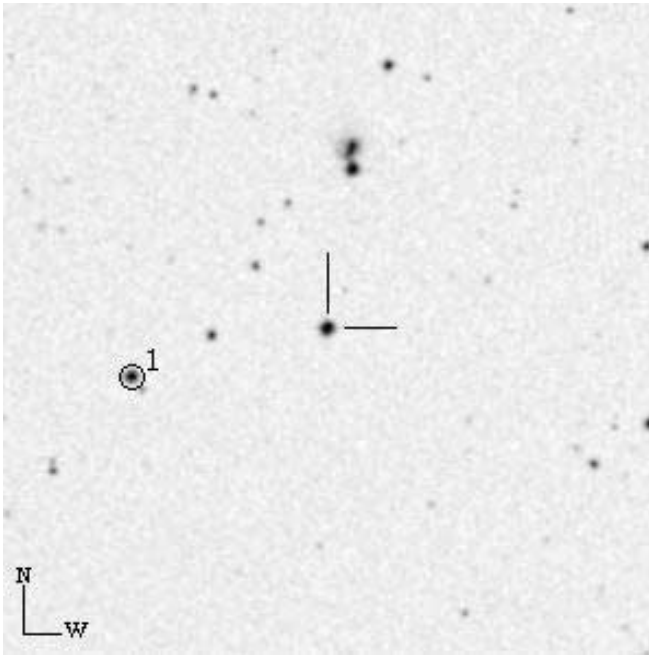
FIG. 3.—Second Generation DSS chart in R ($5' \times 5'$) indicating the position of EC 13471−1258. The comparison star used in the reduction is labelled " 1 ".

obtained spectra using the 300 line mm^{-1} grating blazed at 5000 Å. These spectra were taken on 2002 February 14, March 1, 5, 8–10, 30, 31, and April 1, 5–7, 15. The spectral range of the spectra up to March 10 was 3335 to 6465 Å with a dispersion of 2.846 Å pixel^{-1}, then the grating was tilted to produce spectra with the range of 3850 to 6970 Å with a dispersion of 2.83 Å pixel^{-1}. The exposure times ranged from 10 to 30 minutes, depending on the conditions and the magnitude of the object, followed by an FeAr arc exposure of 120 s and FeNe arc exposure of 5 s. For the flux calibration we used LTT 2415 as the standard. The spectra were reduced using the Image Reduction and Analysis Facility (IRAF).[4]

2.2. Photometry

We have obtained photometric data of BPM 6502 at the 61 cm Perth/Lowell Boller & Chivens Cassegrain reflector (f/13.5) at the Perth Observatory on 2001 October 9, 10 and December 18–23. We have obtained a total of 173 images in I and 170 in R. The exposure times were 120 s for both I and R filters. We have used Apogee AP7 camera, with a 512×512 thinned and back-illuminated CCD. The images are $5' \times 5'$ and have a resolution of $0''.58$ pixel^{-1}.

The images were reduced with DoPHOT (Schechter, Mateo, & Saha 1993) where all stars in the images were measured. A set of seven reference stars were chosen and their fluxes summed to form reference magnitudes for each image for both I and R filters. These were subtracted from each measurement of BPM 6502 to minimize any external effects causing variations between exposures. The overall average

[4] IRAF is distributed by the National Optical Astronomy Observatory, which is operated by the Association of Universities for Research in Astronomy, Inc., under cooperative agreement with the National Science Foundation.

of these differential magnitudes is used as the photometric zero point for the light curve calculated for I and R bands. Figure 1 shows one of the images taken using the R filter with BPM 6502 and the reference stars marked.

Photometry of EC 13471−1258 was conducted at MSO using the 74 inch telescope with the Monash Imager on 2002 April 18, 19, and 21. We used a 2K × 4K CCD camera reduced to 2048 × 2200 and binned 6 × 6, and the B and R filters, with 20 s exposure times. The images are $3'.0 \times 3'.3$ and have a resolution of $0''.546$ per binned pixel. Figure 3 shows the locations of EC 13471−1258 and of the star used to obtain a reference magnitude for EC 13471−1258.

2.3. HST Imaging Spectrograph Observations

D. O'Donoghue observed EC 13471−1258 with the STIS, obtaining four exposures on 1999 August 28. A 600 s exposure was taken using the NUV-MAMA configuration with a spectral coverage of 1568 to 3184 Å and a resolution of 3.4 Å. The G230L filter centered at 2376 Å with a bandwidth of 1616 Å was used. Two more exposures of 1800 s and one of 900 s duration were obtained using the FUV-MAMA configuration with a spectral range of 1140 to 1730 Å and a resolution of 1 Å. For these exposures the G140L filter was centered at 1425 Å with a bandwidth of 590 Å.

3. ANALYSIS

3.1. Spectroscopy

3.1.1. Orbital Parameters

The Hα emission that originates from the red dwarf is used to obtain the red dwarf radial velocities. The Hα emission centroid was measured using IRAF's SPLOT routines. The shift in Hα emission was converted into radial velocities, which were corrected for the Earth's motion. Table 1 gives the Heliocentric Julian Dates with the corresponding heliocentric radial velocities for BPM 6502. The radial velocity measurements of K2000 and from this work were combined to calculate an improved orbital period of the binary system. The updated orbital period is

$$P = 0.336784 \pm 0.000001 \text{ days} ,$$

and the updated epoch of inferior conjunction is

$$T_0 = 2,451,612.810 \pm 0.001 \text{ (HJD)} .$$

Figure 4 (*top*) shows the radial velocity measurements of the red dwarf from K2000 and this paper, folded using the updated period. The semiamplitude of the combined measurements is 71.7 ± 0.9 km s^{-1} with the systemic velocity, $\gamma = 9.2 \pm 0.7$ km s^{-1}. The mass function for BPM 6502 is $0.0129 \pm 0.0005\ M_\odot$. Using Kepler's law, K2000 estimated a system inclination $i = 22° \pm 3°$. At this inclination, reprocessing in the illuminated hemisphere of the late-type star should result in Hα equivalent width (EW) variations of the order of 40% (i.e., ≈sin i) and in phase with the orbit, but K2000 found the measurements to be severely affected by blending with the NLTE absorption core from the white dwarf. We have corrected for this effect by normalizing the observed spectra to a NLTE model spectrum (TLUSTY, Hubeny & Lanz 1995) at $T_{\rm eff} = 22,000$ K and log $g = 8.0$, and shifted to the white dwarf radial velocity (K2000), and we remeasured the EWs. Figure 4 (*second from top*) shows the variation of EWs, which is offset from the radial veloc-

TABLE 1
Hα Radial Velocity Measurements for BPM 6502

HJD (2,452,300+)	V (km s⁻¹)	HJD (2,452,300+)	V (km s⁻¹)	HJD (2,452,300+)	V (km s⁻¹)
1.078935..........	−41.37	2.107636..........	−57.37	17.088010........	73.34
1.102350..........	−50.05	2.130959..........	−58.75	17.110974........	88.86
1.125650..........	−50.52	6.949260..........	47.26	17.134366........	77.87
1.148556..........	−55.11	16.938247........	−55.37	17.157400........	60.49
1.171473..........	−27.72	16.961338........	−54.47	17.180410........	40.83
2.014473..........	45.46	16.984128........	−39.86	17.203987........	−8.52
2.037691..........	14.85	17.007220........	−25.72	17.227078........	−30.93
2.061060..........	−16.21	17.041631........	25.88		
2.084163..........	−40.45	17.064711........	57.83		

ities by 0.28 ± 0.04 phase. The semiamplitude of the variations is 0.51 ± 0.04 Å centered about 2.03 ± 0.03 Å, which corresponds to an inclination of $15° \pm 1°$ using model A in Thorstensen et al. (1978). This suggests that most of the variation is due to the illumination effect and that the Hα emission traces an orbit inferior to the center of mass of the red dwarf.

Radial velocity measurements for BPM 71214 are shown in Table 2. The radial velocity measurements marked with a footnote were measured from low-dispersion spectra. For the calculation of the period these velocities had a reduced weight (0.25) compared with the radial velocities obtained from high-dispersion spectra. Figure 5 shows the periodogram of Hα radial velocity measurements with the velocities folded over the best orbital period of

$$P = 0.20162 \pm 0.00004 \text{ days}$$

and the epoch of inferior conjunction

$$T_0 = 2,452,317.900 \pm 0.005 \text{ (HJD)}.$$

We found the semiamplitude of the red dwarf to be 123.6 ± 2.1 km s⁻¹ and the systemic velocity of the system to be 46.2 ± 1.5 km s⁻¹. The mass function of the white dwarf is $0.039 \pm 0.002 \, M_\odot$, and it differs significantly from the mass function quoted in Livio & Shara (1987) of 0.20, which is therefore in error. The mass function and probable mass of the components (see below) suggest a system inclination of $i \sim 30°$. The Hα EW did not appear to vary over the orbital period (EW ~ 6.0 Å), despite model expectations of about 50% (i.e., $\approx \sin$); therefore we conclude that the Hα emission is due to coronal activity and not to an illumination effect. The Hα emission is most probably distributed over the entire surface of the star, and the inferred orbital

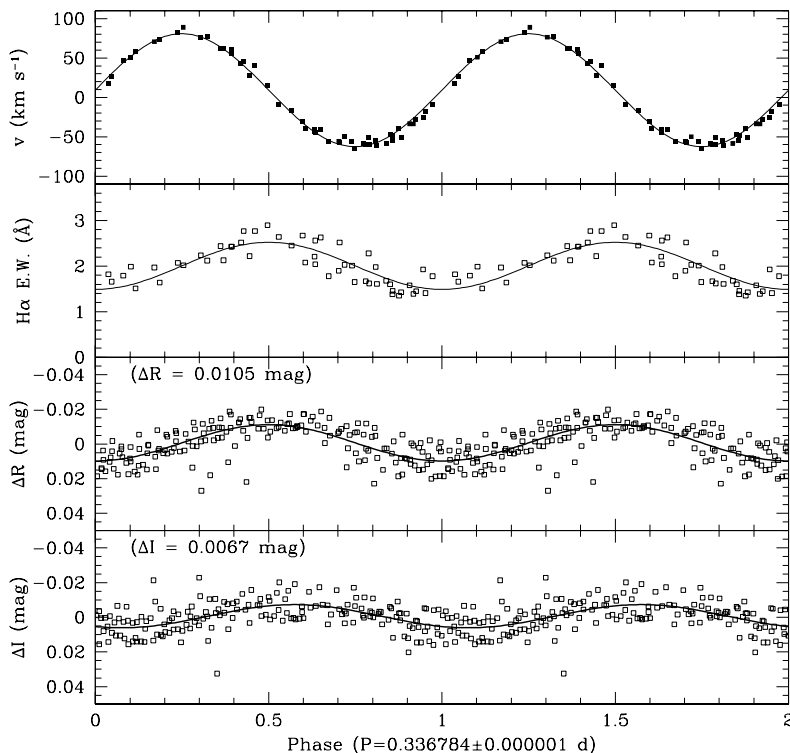

Fig. 4.—Radial velocity measurements, Hα EWs, and photometric variations in *R* and *I* of BPM 6502, folded on the orbital period. Phasing of the photometry and Hα EWs show evidence of the illumination effect of the red companion.

TABLE 2
Hα Radial Velocity Measurements for BPM 71214

HJD (2,452,300+)	V (km s⁻¹)	HJD (2,452,300+)	V (km s⁻¹)	HJD (2,452,300+)	V (km s⁻¹)
17.925971........	149.38	34.966624........	−46.65	41.915241........	119.69
17.939419........	175.85	34.975604........	−72.24	41.925351........	146.63
17.951871........	179.94	34.984817........	−99.65	41.934094........	168.09
17.964359........	163.92	34.993670........	−100.57	41.943017........	167.16
17.977633........	136.50	35.002477........	−55.81	41.952368........	166.24
18.014806........	−6.98	35.910990........	133.57	41.961280........	149.80
18.028230........	−41.25	35.924114........	98.38	41.970168........	129.69
18.041424........	−69.13	35.936671........	71.87	41.980919........	95.43
18.051944........	−60.00	35.949089........	26.17	43.887207........	−21.43
18.956608........	167.64	35.961298........	−13.58	43.899440........	14.64
18.972811........	164.41	38.948822........	145.97	43.911846........	51.17
18.985495........	142.02	38.984097........	0.68	43.921498........	86.79
19.998020........	123.78	40.894593........	79.76	43.934923........	132.46
20.010392........	84.48	40.906918........	124.04	43.951693........	154.82
20.022983........	27.83	40.919324........	154.18	64.865413........	−3.67[a]
20.035355........	−14.67	40.931789........	166.96	64.876663........	29.66[a]
34.901317........	150.77	40.944149........	169.69	64.887878........	47.94[a]
34.913572........	101.42	40.956532........	140.44	64.900562........	80.36[a]
34.927715........	84.95	40.967654........	131.29	65.868576........	−76.40[a]
34.946915........	16.87	41.890683........	34.75	65.880763........	10.84[a]
34.957573........	−21.06	41.902985........	77.22	65.892383........	39.15[a]

[a] Velocity measured from a low-dispersion spectrum.

parameters are representative of the motion of the red dwarf center of mass. We note that the source of X-rays is also probably related to coronal activity. From the estimated mass ratio (∼0.5) and primary mass (0.77 $M_\odot$) we predict a contact period of ∼0.2 days, which suggest that BPM 71214 should already be filling its Roche lobe. Photometric observations should confirm the presence of ellipsoidal variations and the hibernation scenario suggested by Livio & Shara (1987) should be investigated further.

The radial velocity measurements for EC 13471−1258 are shown in Table 3, with Figure 6 showing the radial velocities folded over the best orbital period of
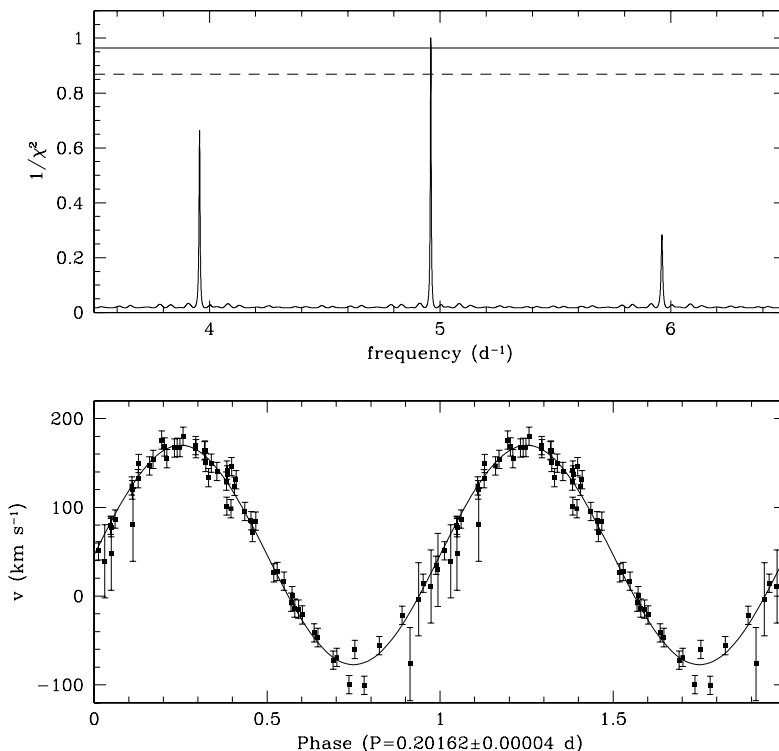
$$P = 0.15074 \pm 0.00004 \text{ days}$$

Fig. 5.—*Bottom*: Velocity of the red dwarf in BPM 71214 traced by Hα and folded on the orbital period and best fit. *Top*: Periodicity analysis. The full line shows the 99% confidence level, and the dashed line the 90% confidence level, of the orbital period.

TABLE 3
Hα Radial Velocity Measurements for EC 13471−1258

HJD (2,452,300+)	V (km s⁻¹)	HJD (2,452,300+)	V (km s⁻¹)	HJD (2,452,300+)	V (km s⁻¹)
35.124219........	100.94	42.178830........	−279.08	43.272388........	146.93
35.140239........	171.24	42.194571........	−73.56	43.284703........	200.35
35.156166........	206.38	42.210325........	152.06	43.296996........	219.05
35.172128........	37.32	42.226148........	325.60	44.051143........	163.98
35.188043........	−61.85	42.246682........	198.10[a]	44.062463........	82.65[a]
35.203959........	−243.70	42.254564........	135.95[a]	64.930889........	−200.17[a]
35.219817........	−256.98	42.266417........	31.77[a]	64.942081........	−150.39[a]
35.235732........	−201.75	42.293108........	−283.95[a]	65.010185........	116.26[a]
35.251521........	−64.76	43.145168........	208.48	65.021968........	64.17[a]
35.267413........	51.69	43.157542........	130.80	65.033496........	−34.08[a]
35.283160........	134.79	43.169834........	39.40	65.044897........	−103.08[a]
42.068162........	157.88	43.182324........	−10.43	65.056182........	−203.60[a]
42.084043........	238.71	43.194570........	−174.45	65.951375........	−260.53[a]
42.099866........	187.51	43.207048........	−257.63	65.962683........	−260.55[a]
42.115747........	22.57	43.219791........	−212.43	65.973887........	−318.57[a]
42.131454........	−102.64	43.234677........	−98.73	65.985207........	−236.82[a]
42.147253........	−260.73	43.247328........	−69.08	70.045329........	−273.65[a]
42.163053........	−290.46	43.260014........	24.08	80.039564........	−9.21[a]

[a] Velocity measured from a low-dispersion spectrum.

with the epoch of inferior conjunction

$$T_0 = 2,452,335.110 \pm 0.006 \ (\mathrm{HJD}) \ .$$

The semiamplitude of the red dwarf is 241.0 ± 8.1 km s⁻¹, and the systemic velocity is -28.1 ± 5.9 km s⁻¹. The mass function for the white dwarf is $0.219 \pm 0.022 \ M_\odot$. We have also observed variations in the Hα emission lines. Most of the Hα emission is related to coronal emission (EW ∼ 5.6

Å), and only a small variable proportion is the result of illumination of the red dwarf by the white dwarf (EW = 0.0–3.6 Å). This means that the orbital parameters are representative of the true center of mass of the system. The Hα emission profile shows two peaks, which could be the result of different temperature distribution on the surface of the red dwarf. The double peaks occur at quadrature where the distortion of the red dwarf is most visible. The Hα EW flared
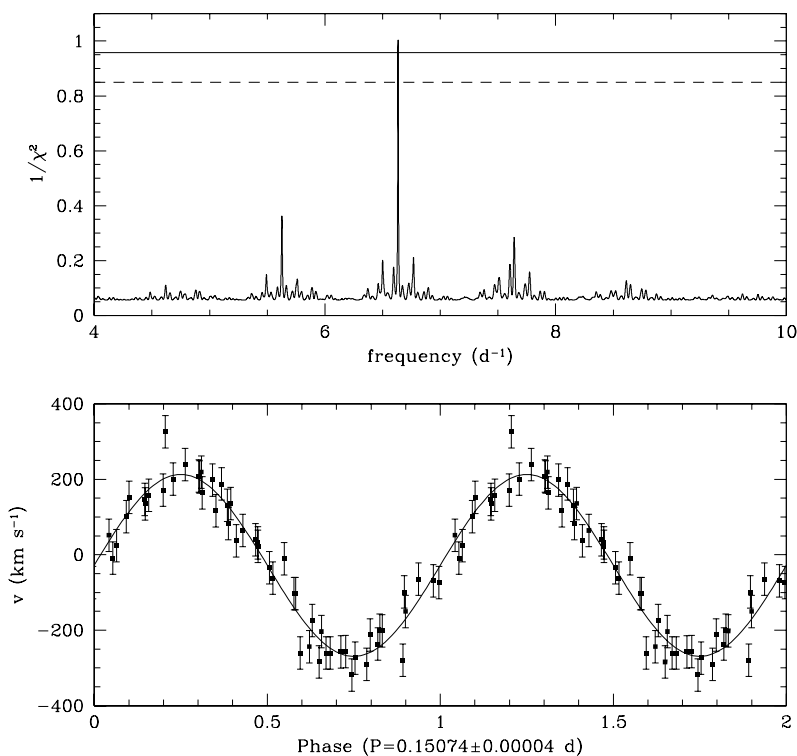

Fig. 6.—Same as Fig. 5, but for EC 13471−1258

TABLE 4
Hα Radial Velocity and EW Measurements for EUVE J0720−31.7

HJD (2,450,000+)	V (km s⁻¹)	EW (Å)	HJD (2,450,000+)	V (km s⁻¹)	EW (Å)
1462.224058	8.32	−2.73	1583.139105	−67.52	−6.38
1493.177829	38.26	−12.77	1583.168491	−66.07	−5.60
1493.207634	21.30	−11.70	1583.193270	−61.98	−4.87
1493.237427	9.18	−11.68	1584.029226	68.71	−12.13
1494.166091	128.53	−7.01	1584.051528	62.08	−11.64
1494.195618	122.27	−7.99	1584.075162	48.78	−11.69
1494.236372	116.19	−8.80	1584.101122	30.78	−11.85
1495.130451	50.69	−2.08	1605.059960	90.83	−2.25
1495.163913	64.98	−2.49	1634.886576	−68.24	−6.80
1496.156503	−56.87	−4.04	1634.938471	−62.00	−5.94
1496.186794	−45.46	−2.69	1635.047748	−45.33	−3.49
1496.216483	−35.61	−2.28	2318.077647	−9.58	−1.93
1496.241913	−30.77	−2.08	2320.062794	40.21	−12.57
1498.243355	30.68	−11.90	2320.089333	23.44	−12.60
1579.102094	0.73	−12.66	2320.112341	16.28	−12.14
1579.125635	−10.09	−12.24	2320.135547	2.58	−10.99
1582.075665	−26.35	−2.82	2320.158463	−10.39	−11.77
1582.099357	−15.34	−2.56	2320.181275	−22.92	−12.28
1582.122365	−2.01	−2.04	2320.204191	−26.64	−10.41
1583.064893	−54.03	−8.57	2320.227327	−41.83	−11.33
1583.112161	−67.06	−6.85			
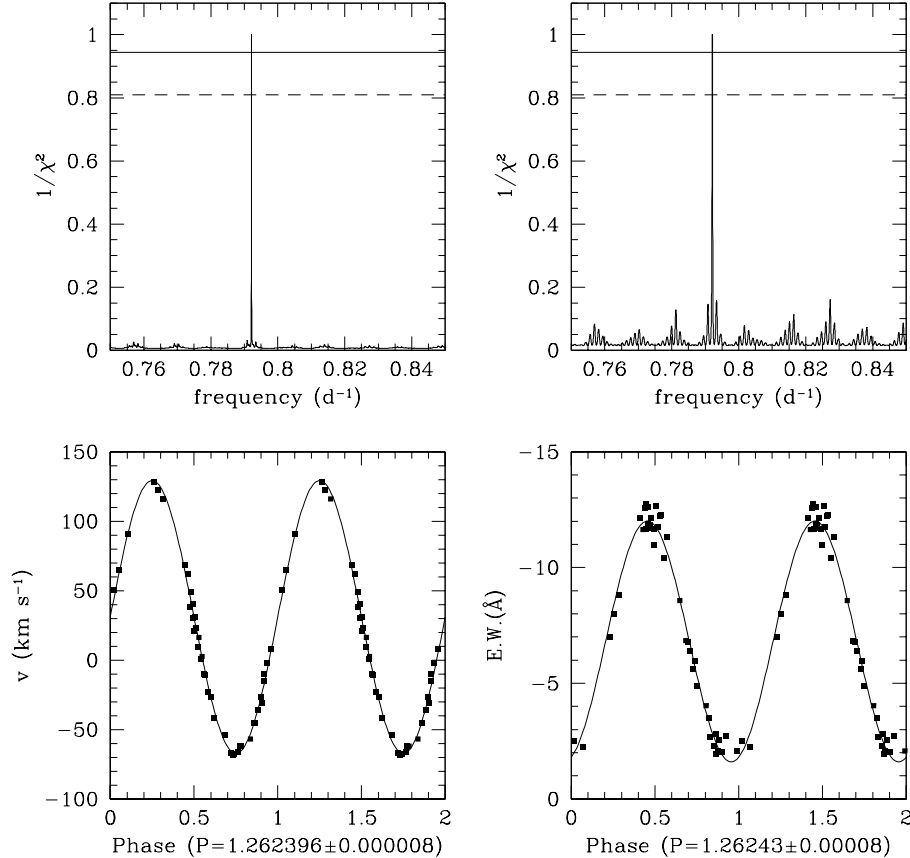
Fig. 7.—*Bottom left*: Velocity of the red dwarf in EUVE J0720−31.7, traced by Hα and folded on the orbital period of 1.262396 days. *Top left*: Periodicity analysis. *Bottom right*: Hα EWs phased on the orbital period estimated from these measurements (1.26243 days). *Top right*: Periodicity analysis. The EWs show a phase offset from the radial velocity measurements $\Delta\Phi = 0.29 \pm 0.03$, close to the predicted offset of 0.25.

to 17 Å on UT 2002 March 8, indicative, along with the noted X-ray emission, of strong coronal activity.[5]

We have measured the radial velocity of the white dwarf from the STIS spectra, where the extreme velocity difference is 309 ± 70 km s^{-1}. The difference in phase of the measurements is 0.4 to 0.6 phases; therefore the measured velocity amplitude sets the minimum amplitude for the white dwarf. On the other hand, the predicted semiamplitude of the white dwarf calculated from the semiamplitude of the red-dwarf and the mass ratio is 165 ± 35 km s^{-1}, which suggests that the STIS spectra were observed near quadrature where the maximum velocities occur, and $q \leq 0.79$.

Table 4 shows the radial velocity and EW measurements of EUVE J0720−31.7. Figure 7 shows the radial velocities folded over the period with the periodogram clearly showing the best period. The best orbital period for this system is

$$P = 1.262396 \pm 0.000008 \text{ days} ,$$

with the epoch of inferior conjunction

$$T_0 = 2,451,462.277 \pm 0.003 \text{ (HJD)} .$$

The semiamplitude of the red dwarf is 98.2 ± 1.2 km s^{-1} and the systemic velocity is 31.1 ± 0.7 km s^{-1}. A search for the best period using the EW measurements resulted in a period of

$$P = 1.26243 \pm 0.00008 \text{ days}$$

with the epoch of minimum emission

$$T_0 = 2,451,461.906 \pm 0.027 \text{ (HJD)} .$$

This period agrees with the period obtained from radial velocities within the uncertainties. The EUV illumination model (Thorstensen et al. 1978) predicts that the maximum emission-line strength lags the maximum radial velocity by 0.25 phase compared with our measured offset of 0.29 ± 0.03. The Hα EWs vary with a semiamplitude of 5.24 ± 0.10 Å centered about -6.81 ± 0.08 Å, which results in an inclination of $50° \pm 2°$ using model A from Thorstensen et al. (1978). The mass function from these data is 0.1239 ± 0.0045, which is in agreement with Vennes & Thorstensen (1996).

3.1.2. *Spectral Decomposition*

A clean white dwarf spectrum may be obtained by subtracting a series of late-type spectra from the observed low-dispersion spectrum until the TiO bands are not observed from the resulting spectrum. Pickles (1998) provides a library of spectra that represent M-type stars. To analyze the white dwarfs, a grid of convective pure-H model atmospheres was computed using a new version of the Mihalas, Auer, & Heasley (1975) computer code modified to include convection within the existing numerical treatment. This new grid extends toward lower temperatures a previous grid of LTE DA models used by Vennes (1999) in a study of X-ray selected white dwarfs, and it now covers the effective
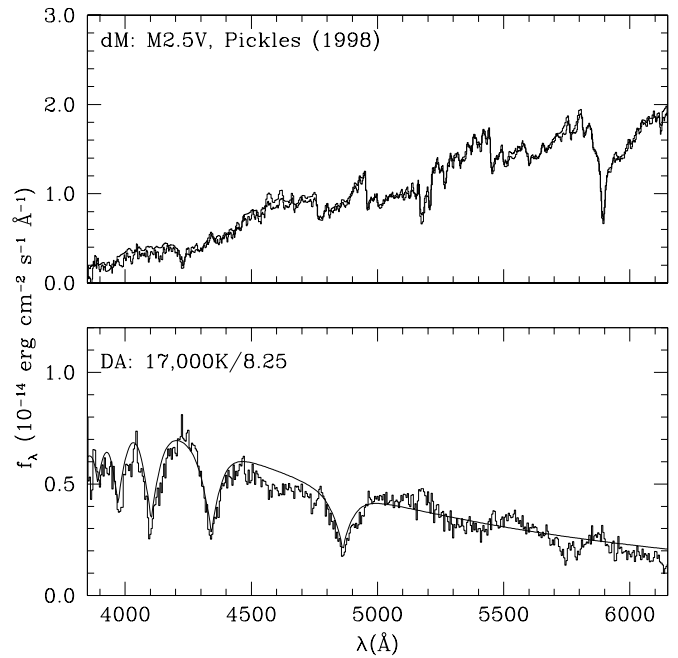

FIG. 8.—Decomposed spectrum of BPM 71214 showing the spectrum of the red dwarf (*top*) compared with a dM2.5 template from Pickles (1998), and of the white dwarf (*bottom*) compared with a model spectrum at $T_{\rm eff} = 17,000$ K and $\log g = 8.25$.

temperatures from 7000 to 84,000 K and surface gravities from $\log g = 7.0$ to 9.5. Detailed Stark-broadened synthetic line profiles are computed based on the converged model structures. A separate grid of synthetic spectra was computed, which includes the effect of Lyα satellites (see Allard & Koester 1992).

Figure 8 shows the decomposed spectra of the white dwarf and the red dwarf in BPM 71214, based on a series of low-dispersion spectra. We found the spectral type of the red dwarf to be M2.5 V, and we compared the resulting white dwarf spectrum with a grid of model spectra to obtain $T_{\rm eff} = 17200 \pm 1000$ K and $\log g = 8.20 \pm 0.10$. Figure 9 (*right*) shows the Balmer lines of the white dwarf after decomposition compared with the best-fit synthetic spectrum with confidence contours for the fit. The mass of the white dwarf is 0.77 ± 0.06 $M_\odot$ with a cooling age of $2.15 \pm 0.37 \times 10^8$ yr, which has been calculated using Wood (1995) models.

We obtained low-dispersion spectra of EUVE J0720−31.7 on two separate nights. We determined the temperature and surface gravity by comparing each spectrum with the grid of models with the contribution of Hε both included and excluded because of its lower signal-to-noise ratio. We have also excluded the core of Hβ (± 12 Å) because of the presence of emission. The average and standard deviation of all four measurements provide an effective temperature of $T_{\rm eff} = 55,550 \pm 1360$ K and a surface gravity of $\log g = 7.74 \pm 0.07$. These uncertainties are more accurate representations of the errors in temperature and surface gravity than fitting errors only. Next we subtracted the spectrum GL 218 (M1.5) such that the TiO bands were no longer observed. The two subtracted spectra of EUVE J0720−31.7 were then compared with the grid of model spectra, again including and excluding Hε, to obtain a mean of $T_{\rm eff} = 53,900 \pm 1770$ K and $\log g = 7.83 \pm 0.08$. The

---

[5] The red dwarf X-ray luminosities in BPM 71214 and EC 13471−1258 have been estimated to be 1.2 and 1.6×10^{29} erg s^{-1}, respectively, assuming distances of 68 and 55 pc, respectively. X-ray count rates are converted to fluxes following Voges et al. (1999). The ratio of the X-ray to bolometric luminosities ($\log L_{\rm X}/L_{\rm bol} \gtrsim -3$) and Rossby numbers ($\log R_0 \lesssim -2.1$) places these stars at a critical location for the study of coronal activity (see James et al. 2000 and Christian & Mathioudakis 2002).
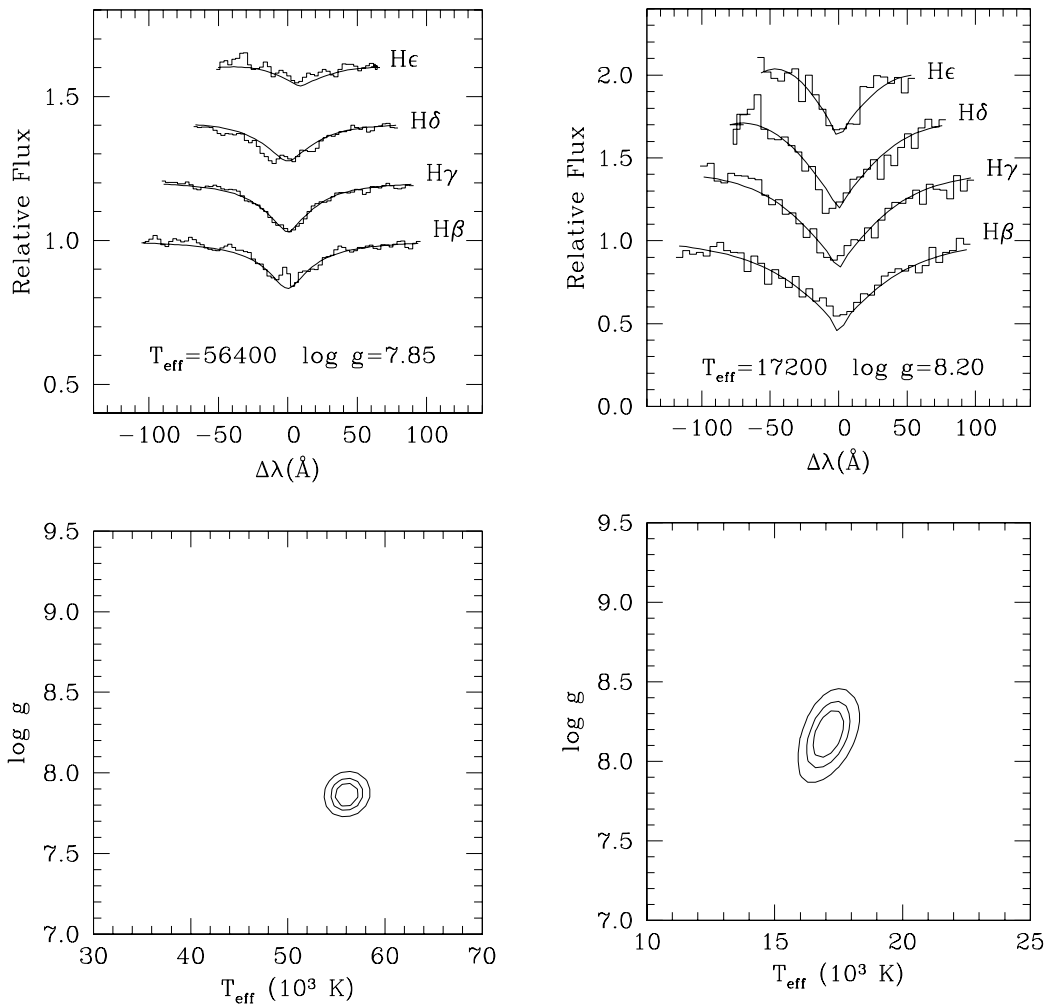
Fig. 9.—Balmer line profiles EUVE J0720−31.7 compared with model spectra at 56,400 K and log g = 7.85 (*top left*), and of BPM 71214 at T_{eff} = 17,200 K and log g = 8.20 (*top right*), with their respective confidence contours at 66%, 90%, and 99% (*bottom*).

effect of subtracting the contribution of the red dwarf is a lower temperature and a higher gravity. Figure 9 (*left*) shows the Balmer lines of EUVE J0720−31.7 from one of the subtracted spectrum compared with a grid of model spectra, along with the confidence contours for the fit.

Figure 10 shows the spectrum of the red dwarf in EC 13471−1258, which was observed during the eclipse. The spectra obtained during the eclipse were combined and then subtracted from noneclipsing spectra obtained shortly before and after the eclipse, resulting in a spectrum for the white dwarf. We compared this spectrum with a grid of model spectra to obtain an effective temperature of 14,200 ± 500 K and log g = 8.15 ± 0.15. Because of the Balmer line emission, the line cores (±12 Å) were excluded from the fit. We have also compared the *HST* data with the same grid of models to obtain an effective temperature of 14,080 ± 100 K and log g = 8.26 ± 0.05. Therefore the two measurements are in agreement. Figure 11 shows the comparisons of the STIS and optical data with the models with their respective confidence contours. The STIS spectrum clearly shows Lyα satellite features near 1400 and 1600 Å first introduced by Allard & Koester (1992) in the study of variable ZZ Ceti stars. Figure 12 shows the STIS and low-dispersion optical spectra compared with a model spectrum at T_{eff} = 14,080 K and log g = 8.26; the red dwarf contribu-
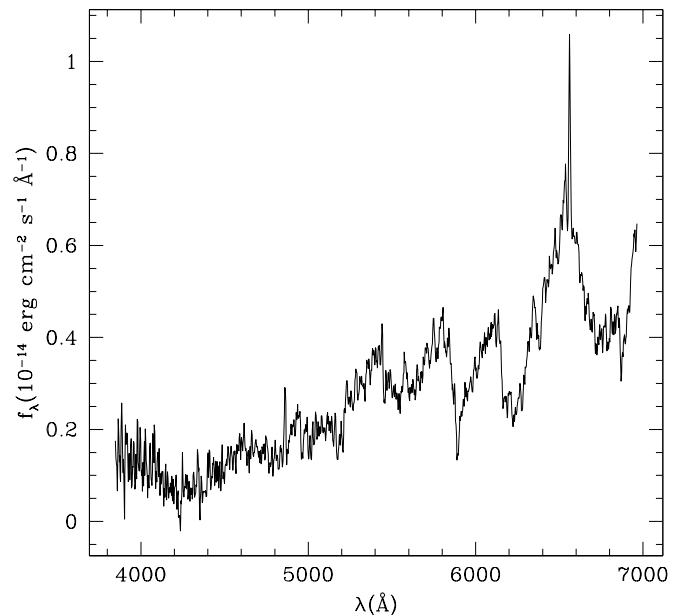
Fig. 10.—Spectrum of the red dwarf in EC 13471−1258 observed while the white dwarf was being eclipsed by the red dwarf.
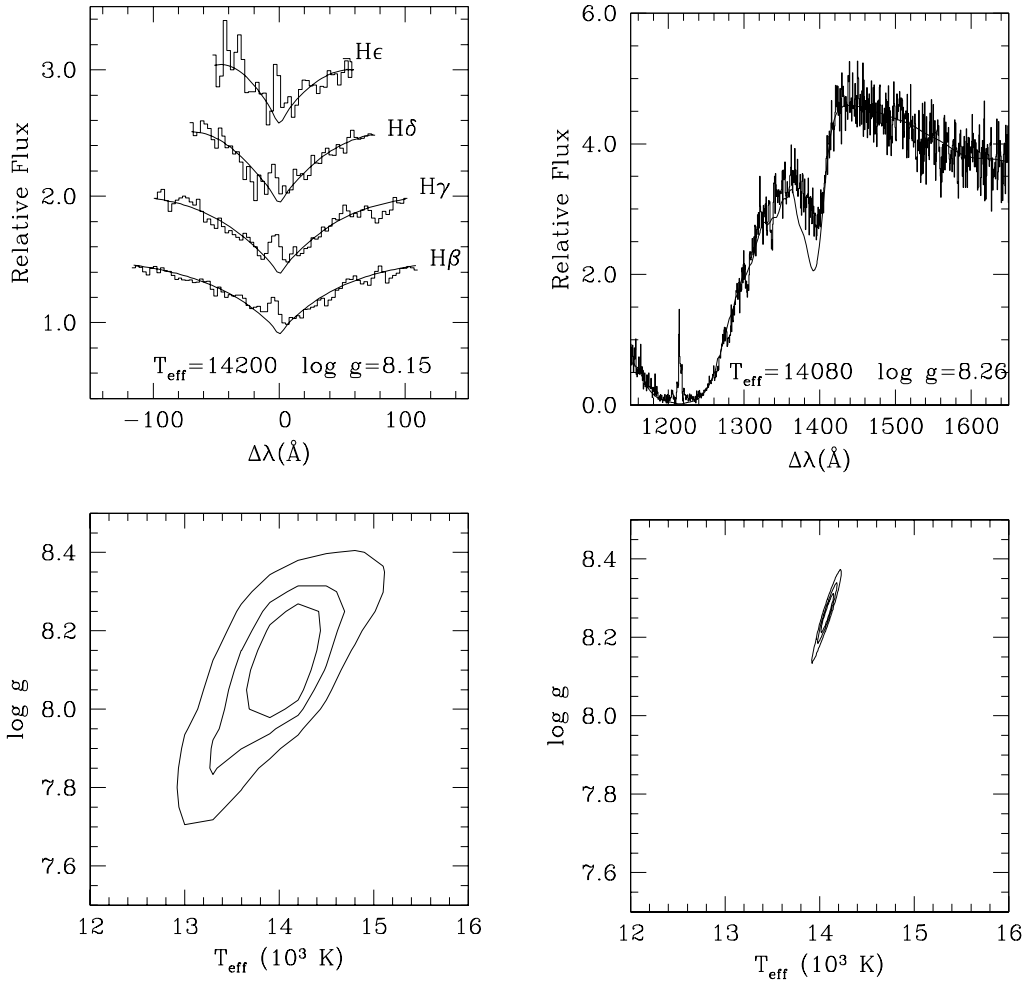
FIG. 11.—Balmer lines and Lyman β of the white dwarf in EC 13471−1258 compared with model spectra at 14,200 K and log $g = 8.15$ (*top left*), and 14,080 K and log $g = 8.15$ (*top right*), with their respective confidence contours at 66%, 90%, and 99% (*bottom*).

tion can be clearly seen at longer wavelengths. The mass of the white dwarf is 0.77 ± 0.04 $M_\odot$ with a cooling age of $3.75 \pm 0.25 \times 10^8$ yr, which has been calculated using Wood (1995) models.

We have measured the Hα FWHM in the high-resolution spectra and calculated the rotational velocity of the red dwarf in EC 13471−1258. We subtracted in quadrature the intrinsic width of the emission lines, which we took as 1.7 Å (Houdebine & Doyle 1994), the resolution of 1.7 Å and the broadening due to the orbital motion of the secondary. The FWHM due to rotational broadening is 5.3 ± 1.0 Å, which corresponds to $v \sin i = 140 \pm 28$ km s^{-1}. Assuming that the red companion is tidally locked to the white dwarf, the radius of the companion is 0.42 ± 0.08 $R_\odot$. Note that our estimate is only indirect and may be influenced by unknown systematic effects.

3.2. Photometry
3.2.1. BPM 6502

Photometric variations with amplitudes of 0.0105 and 0.0067 mag in R and I, respectively, were observed in BPM 6502. Figure 4 shows the I and R photometric measurements folded over the spectroscopic period. The average error of the photometric measurements is 0.006 mag. The photometric maximum lags the velocity maximum by 0.25

FIG. 12.—STIS and low-dispersion spectra of EC 13471−1258 compared with a model spectrum at $T_{eff} = 14,080$ K and log $g = 8.26$.

TABLE 5A

Photometric Measurements in R for EC 13471−1258

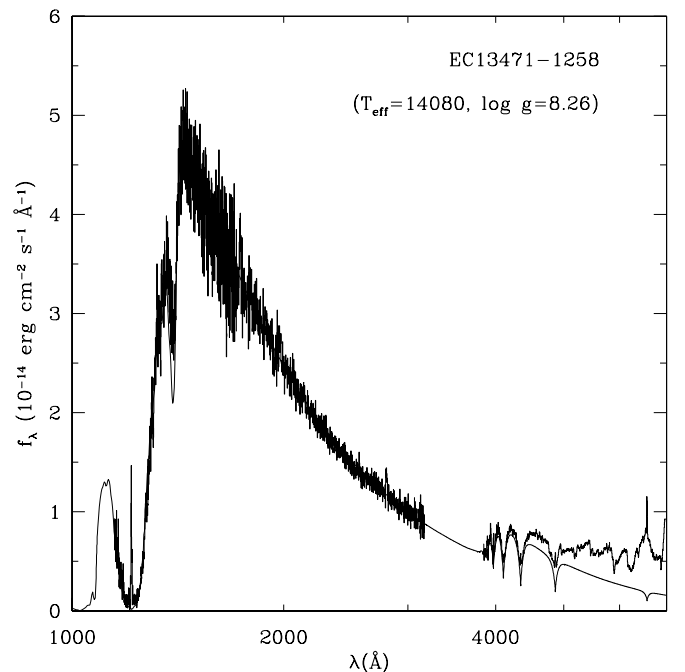| HJD[a]	ΔR	HJD[a]	ΔR	HJD[a]	ΔR	HJD[a]	ΔR	HJD[a]	ΔR
4.14255	−0.072	4.17732	0.099	4.21269	−0.116	4.24812	0.052	4.28424	−0.014
4.14345	−0.090	4.17805	0.104	4.21342	−0.108	4.24883	0.066	4.28569	−0.078
4.14417	−0.086	4.17876	0.097	4.21415	−0.111	4.24957	0.083	4.28786	−0.045
4.14489	−0.073	4.17948	0.097	4.21486	−0.123	4.25027	0.356	4.29003	−0.039
4.14560	−0.084	4.18019	0.100	4.21558	−0.106	4.25099	0.371	4.29145	−0.088
4.14632	−0.066	4.18092	0.107	4.21630	−0.111	4.25173	0.388	4.29219	−0.044
4.14705	−0.075	4.18165	0.096	4.21702	−0.109	4.25244	0.380	4.29291	−0.163
4.14777	−0.075	4.18235	0.088	4.21774	−0.114	4.25315	0.395	4.29362	−0.091
4.14848	−0.072	4.18308	0.093	4.21847	−0.110	4.25389	0.382	4.29436	−0.084
4.14921	−0.071	4.18381	0.081	4.21918	−0.112	4.25460	0.357	6.06677	0.406
4.14994	−0.073	4.18452	0.093	4.21990	−0.105	4.25532	0.386	6.06748	0.389
4.15064	−0.072	4.18525	0.087	4.22063	−0.111	4.25606	0.405	6.06819	0.409
4.15137	−0.051	4.18598	0.080	4.22136	−0.100	4.25678	0.401	6.06892	0.393
4.15210	−0.049	4.18674	0.070	4.22207	−0.100	4.25748	0.377	6.06964	0.090
4.15281	−0.056	4.18746	0.071	4.22279	−0.103	4.25821	0.402	6.07036	0.091
4.15355	−0.044	4.18819	0.054	4.22351	−0.120	4.25894	0.369	6.07107	0.094
4.15427	−0.047	4.18962	0.057	4.22424	−0.104	4.25965	0.396	6.07179	0.085
4.15498	−0.039	4.19034	0.056	4.22495	−0.099	4.26036	0.069	6.07268	0.076
4.15571	−0.036	4.19106	0.045	4.22569	−0.089	4.26111	0.075	6.07341	0.077
4.15643	−0.027	4.19179	0.040	4.22641	−0.065	4.26181	0.092	6.07413	0.072
4.15713	−0.024	4.19249	0.032	4.22711	−0.092	4.26253	0.053	6.07483	0.069
4.15786	−0.014	4.19321	0.031	4.22783	−0.059	4.26327	0.066	6.07556	0.074
4.15857	−0.017	4.19394	0.025	4.22856	−0.070	4.26398	0.054	6.07628	0.067
4.15931	−0.012	4.19466	0.019	4.22928	−0.097	4.26469	0.067	6.07699	0.066
4.16003	−0.001	4.19538	0.009	4.23009	−0.068	4.26543	0.084	6.07772	0.051
4.16073	0.002	4.19610	−0.001	4.23080	−0.083	4.26615	0.044	6.07843	0.065
4.16146	−0.006	4.19683	−0.018	4.23152	−0.050	4.26686	0.055	6.07914	0.056
4.16219	0.022	4.19754	−0.026	4.23297	−0.060	4.26760	0.050	6.07986	0.051
4.16290	0.016	4.19827	−0.024	4.23370	−0.045	4.26832	0.023	6.08059	0.053
4.16363	0.020	4.19899	−0.026	4.23440	−0.050	4.26902	0.029	6.08130	−0.031
4.16436	0.025	4.19973	−0.040	4.23513	−0.034	4.26975	0.004	6.08201	0.040
4.16507	0.020	4.20043	−0.044	4.23586	−0.040	4.27048	0.059	6.08274	0.031
4.16578	0.030	4.20115	−0.049	4.23657	−0.015	4.27119	0.034	6.08346	0.034
4.16651	0.044	4.20188	−0.053	4.23729	−0.016	4.27190	0.062	6.08419	0.030
4.16724	0.038	4.20260	−0.061	4.23801	−0.007	4.27264	0.008	6.08490	0.018
4.16795	0.054	4.20333	−0.074	4.23873	0.029	4.27343	−0.012	6.08562	0.008
4.16869	0.065	4.20404	−0.061	4.23946	0.017	4.27489	−0.008	6.08634	0.025
4.16940	0.072	4.20476	−0.072	4.24017	0.011	4.27560	−0.007	6.08705	0.025
4.17011	0.063	4.20548	−0.073	4.24090	0.006	4.27631	0.005	6.08777	0.006
4.17085	0.081	4.20621	−0.081	4.24161	0.016	4.27705	0.017	6.08849	−0.005
4.17157	0.083	4.20692	−0.090	4.24233	0.000	4.27777	0.009	6.08920	−0.003
4.17227	0.071	4.20764	−0.090	4.24306	0.007	4.27848	−0.036	6.08993	−0.034
4.17300	0.102	4.20837	−0.080	4.24378	0.055	4.27920	−0.009	6.09064	−0.024
4.17373	0.087	4.20910	−0.095	4.24450	0.042	4.27994	0.004	6.09135	−0.034
4.17444	0.090	4.20981	−0.100	4.24523	0.045	4.28136	−0.032	6.09207	−0.047
4.17517	0.085	4.21053	−0.105	4.24595	0.045	4.28210	−0.102	6.09279	−0.022
4.17589	0.096	4.21126	−0.105	4.24666	0.065	4.28282	−0.009	6.09351	−0.052
4.17660	0.097	4.21198	−0.108	4.24739	0.060	4.28352	−0.111	6.09423	−0.046
6.09494	−0.045								
6.09567	−0.058								
6.09637	−0.050								
6.09710	−0.060								
6.09782	−0.055								
6.09855	−0.086								
6.09927	−0.080								
6.09998	−0.076								
6.10069	−0.075								
6.10141	−0.056								
6.10214	−0.078								
6.10286	−0.087								
6.10356	−0.106								
6.10428	−0.091								
6.10500	−0.090								
6.10571	−0.081								
6.10642	−0.067								
6.10715	−0.078								
6.10787	−0.076								
6.10858	−0.060								
6.10930	−0.060								
6.11003	−0.088								
6.11075	−0.078								
6.11147	−0.036								
6.11217	−0.045								
6.11289	−0.078								
6.11362	−0.046								
6.11433	−0.035								
6.11504	−0.033								
6.11604	−0.026								
6.11674	−0.021								
6.11746	−0.025								
6.11818	−0.005								
6.11890	−0.013								
6.11961	−0.006								
6.12033	0.006								
6.12105	−0.006								
6.12176	0.000								
6.12248	−0.002								
6.12320	0.039								
6.12390	0.023								
6.12463	0.012								
6.12607	0.064								
6.12678	0.051								
6.12751	0.054								
6.12821	0.076								
6.12894	0.068								
6.13252	0.136								

a HJD 2,452,380+.

TABLE 5B

PHOTOMETRIC MEASUREMENTS IN R FOR EC 13471−1258

HJD[a]	ΔR	HJD[a]	ΔR	HJD[a]	ΔR	HJD[a]	ΔR	HJD[a]	ΔR	HJD[a]	ΔR
6.13394	0.104	6.16503	−0.090	6.18871	−0.070	6.20987	0.357	6.22994	0.054	6.26674	−0.095
6.13466	0.095	6.16574	−0.125	6.18944	−0.064	6.21059	0.413	6.23066	0.062	6.26745	−0.046
6.13539	0.100	6.16717	−0.083	6.19015	−0.045	6.21129	0.402	6.23139	0.069	6.26817	−0.037
6.14687	0.081	6.16789	−0.109	6.19088	−0.052	6.21201	0.409	6.23282	0.026	6.26890	−0.044
6.14758	0.079	6.16862	−0.139	6.19158	−0.052	6.21272	0.396	6.23353	0.036	6.26960	−0.059
6.14831	0.060	6.16935	−0.119	6.19231	−0.045	6.21345	0.424	6.23424	0.026	6.27033	−0.035
6.14902	0.073	6.17005	−0.121	6.19302	−0.053	6.21417	0.414	6.23496	0.031	6.27105	0.027
6.14974	0.058	6.17078	−0.061	6.19373	−0.036	6.21488	0.416	6.23568	0.018	6.27174	0.026
6.15046	0.061	6.17221	−0.105	6.19445	−0.033	6.21561	0.412	6.23640	0.020	6.27247	0.008
6.15117	0.040	6.17292	−0.117	6.19516	−0.017	6.21632	0.421	6.23713	0.023	6.27319	0.029
6.15189	0.038	6.17363	−0.119	6.19589	−0.019	6.21702	0.415	6.23784	0.007	6.27390	0.039
6.15260	0.035	6.17435	−0.121	6.19662	−0.017	6.21775	0.401	6.23855	−0.007	6.27463	0.013
6.15332	0.012	6.17508	−0.121	6.19732	0.000	6.21847	0.413	6.23927	−0.008	6.27533	0.077
6.15404	0.037	6.17580	−0.104	6.19804	0.006	6.21919	0.414	6.24000	−0.003	6.27606	0.067
6.15475	0.017	6.17652	−0.134	6.19877	0.020	6.21990	0.251	6.24071	−0.013	6.27678	0.032
6.15548	0.012	6.17723	−0.142	6.19948	0.030	6.22062	0.091	6.24143	−0.036	6.27748	0.046
6.15620	−0.006	6.17794	−0.103	6.20020	0.023	6.22133	0.079	6.24214	−0.017	6.27820	0.012
6.15692	0.011	6.17867	−0.145	6.20092	0.016	6.22204	0.090	6.24287	−0.028	6.27893	0.035
6.15764	−0.026	6.17938	−0.104	6.20163	0.047	6.22275	0.091	6.24360	−0.054	6.27964	0.064
6.15835	−0.017	6.18010	−0.049	6.20340	0.041	6.22348	0.096	6.24430	−0.044	6.28036	0.077
6.15929	−0.007	6.18298	−0.076	6.20412	0.062	6.22421	0.100	6.24503	−0.059	6.28108	0.082
6.16000	−0.041	6.18369	−0.111	6.20485	0.061	6.22492	0.079	6.24575	−0.069	6.28180	0.047
6.16073	−0.028	6.18441	−0.098	6.20556	0.060	6.22563	0.068	6.26244	−0.072	6.28252	0.119
6.16144	−0.041	6.18511	−0.107	6.20627	0.061	6.22635	0.087	6.26316	−0.078	6.28324	0.060
6.16216	−0.042	6.18584	−0.084	6.20699	0.078	6.22706	0.077	6.26387	−0.048		
6.16288	−0.058	6.18655	−0.076	6.20772	0.075	6.22779	0.062	6.26459	−0.083		
6.16360	−0.054	6.18728	−0.094	6.20842	0.066	6.22849	0.062	6.26531	−0.028		
6.16431	−0.057	6.18799	−0.055	6.20915	0.075	6.22922	0.092	6.26601	0.010		

a HJD 2,452,380+.

2864

TABLE 6

PHOTOMETRIC MEASUREMENTS IN B FOR EC 13471−1258

HJD[a]	ΔB	HJD[a]	ΔB	HJD[a]	ΔB	HJD[a]	ΔB	HJD[a]	ΔB	HJD[a]	ΔB
3.10262	−0.022	3.14154	0.002	3.17625	−0.013	3.21383	−0.020	3.24849	−0.003	4.09249	0.016
3.10332	−0.025	3.14226	−0.026	3.17697	0.000	3.21455	0.043	3.24919	−0.021	4.09395	0.035
3.10404	−0.014	3.14299	−0.013	3.17768	0.002	3.21527	0.045	3.24992	−0.039	4.09467	0.023
3.10550	0.001	3.14369	−0.027	3.17840	0.005	3.21600	0.018	3.25065	0.003	4.09538	0.022
3.10620	0.008	3.14442	−0.039	3.17913	0.005	3.21671	0.018	3.25209	−0.033	4.09610	0.036
3.10693	0.008	3.14514	−0.029	3.17984	0.064	3.21743	0.007	3.25281	−0.032	4.09682	0.032
3.10765	−0.003	3.14597	−0.032	3.18057	0.000	3.21814	0.003	3.25353	0.051	4.09755	0.023
3.10910	0.010	3.14742	−0.014	3.18130	0.010	3.21887	−0.013	3.25425	−0.010	4.09826	0.034
3.10980	−0.011	3.14813	−0.021	3.18200	0.019	3.21960	0.010	3.25498	−0.027	4.09898	0.422
3.11055	0.009	3.14886	−0.035	3.18273	0.008	3.22030	−0.001	3.25570	−0.034	4.10114	1.880
3.11198	0.001	3.14958	−0.040	3.18346	0.003	3.22103	0.012	3.25643	−0.002	4.10188	1.885
3.11271	0.027	3.15029	−0.015	3.18417	0.004	3.22176	−0.026	3.25714	−0.021	4.10260	1.878
3.11343	−0.047	3.15102	−0.020	3.18490	0.016	3.22248	0.030	3.25785	−0.029	4.10330	1.887
3.11414	0.015	3.15175	−0.021	3.18563	0.006	3.22318	0.002	3.25858	−0.013	4.10403	1.882
3.11487	0.016	3.15246	−0.018	3.18633	0.023	3.22391	0.017	3.25931	−0.007	4.10476	1.866
3.11559	0.004	3.15318	−0.029	3.18706	0.021	3.22464	0.022	3.26003	−0.015	4.10547	1.903
3.11631	−0.007	3.15390	−0.026	3.18779	0.020	3.22535	−0.001	3.26074	−0.021	4.10619	1.893
3.11703	0.011	3.15462	−0.045	3.18850	0.013	3.22608	0.010	3.26146	0.011	4.10693	1.874
3.11773	0.000	3.15533	−0.029	3.18931	0.018	3.22681	−0.016	3.26218	0.013	4.10763	1.863
3.11846	0.033	3.15605	−0.029	3.19004	0.010	3.22752	−0.011	3.26291	0.017	4.10836	1.903
3.11919	−0.054	3.15678	−0.045	3.19074	0.033	3.22824	−0.011	3.26361	0.017	4.10909	1.625
3.12136	−0.004	3.15749	−0.034	3.19147	−0.002	3.22895	−0.004	3.26434	0.040	4.10980	0.031
3.12280	0.014	3.15822	−0.043	3.19508	1.830	3.22968	−0.011	3.26507	−0.006	4.11051	0.042
3.12351	0.014	3.15895	−0.053	3.19579	1.878	3.23041	−0.011	3.26578	0.008	4.11197	0.046
3.12497	0.016	3.15967	−0.046	3.19652	1.944	3.23111	0.001	3.26651	0.031	4.11269	−0.017
3.12568	0.023	3.16038	−0.036	3.19725	1.868	3.23184	0.018	3.26724	−0.004	4.11342	0.007
3.12640	0.006	3.16183	−0.020	3.19795	1.854	3.23263	0.009	3.26794	0.056	4.11413	0.013
3.12711	0.016	3.16255	−0.039	3.19941	1.861	3.23334	−0.009	3.26867	0.002	4.11484	−0.001
3.12784	0.015	3.16325	−0.046	3.20012	1.885	3.23406	−0.002	3.26940	−0.005	4.11556	0.023
3.12855	0.008	3.16398	−0.034	3.20085	1.859	3.23479	−0.024	3.27012	0.049	4.11629	0.010
3.12927	0.032	3.16471	−0.050	3.20229	1.896	3.23623	−0.026	3.27084	0.086	4.11701	−0.011
3.13000	0.014	3.16543	0.007	3.20301	1.897	3.23696	−0.028	3.27299	0.048	4.11774	0.017
3.13071	0.010	3.16616	−0.034	3.20374	1.917	3.23768	−0.017	3.27515	0.039	4.11845	0.005
3.13145	0.002	3.16688	−0.023	3.20446	1.806	3.23838	−0.008	4.08301	−0.003	4.11917	−0.006
3.13215	0.020	3.16759	−0.041	3.20516	0.061	3.23911	−0.025	4.08386	0.010	4.11990	0.016
3.13287	0.003	3.16832	−0.031	3.20589	0.037	3.23984	−0.015	4.08458	0.007	4.12062	0.013
3.13361	0.018	3.16903	−0.019	3.20662	0.030	3.24055	−0.015	4.08531	0.001	4.12134	0.019
3.13433	0.009	3.16976	−0.027	3.20733	0.081	3.24128	−0.005	4.08601	0.008	4.12207	0.020
3.13504	0.021	3.17049	−0.012	3.20806	0.043	3.24200	−0.057	4.08674	0.014	4.12278	0.000
3.13649	0.014	3.17121	−0.024	3.20879	0.019	3.24271	−0.012	4.08747	0.013	4.12350	0.014
3.13721	0.003	3.17192	−0.009	3.20949	0.030	3.24344	−0.021	4.08818	0.031	4.12423	−0.003
3.13793	0.002	3.17264	−0.001	3.21022	0.025	3.24417	−0.038	4.08891	0.015	4.12495	0.010
3.13866	−0.011	3.17335	−0.004	3.21095	0.022	3.24487	−0.014	4.08963	0.028	4.12568	0.018
3.13938	−0.017	3.17409	−0.015	3.21167	0.033	3.24559	−0.030	4.09035	0.018	4.12639	−0.004
3.14009	−0.008	3.17480	−0.001	3.21239	0.037	3.24703	−0.009	4.09107	0.021		
3.14082	−0.007	3.17552	0.009	3.21310	0.007	3.24777	−0.044	4.09179	0.019		

[a] HJD 2,452,380+.

phases as expected from an illumination effect. The red dwarf is illuminated by incoming EUV/FUV radiation from the white dwarf, and the projected area toward the line of sight of the illuminated hemisphere varies along the orbit, causing the apparent variability.

3.2.2. *EC 13471−1258*

Tables 5A, 5B, and 6 give the relative photometry of EC 13471−1258 in the *B* and *R* bands. Figure 13 shows the eclipse of the white dwarf in EC 13471−1258 in the *B* and *R* bands, which has been phased with the spectroscopic period. The depth of the eclipse is 0.3 mag in *R* and 1.87 mag in *B*, which shows that the red dwarf companion contributes 24% of the luminosity in *B* and 82% in *R*. The duration of the eclipse is 15.4 minutes, from which we calculated the inclination of the binary using the secondary radius determined from the FWHM of the Hα emission of 0.42 ± 0.08 $R_{\odot}$. The inclination of the system EC 13471−1258 is

$$i = 73.5 \pm 1°1 .$$

We found the mass of the red dwarf companion to be 0.58 ± 0.05 $M_{\odot}$ from the mass function, the inclination, and the mass of the white dwarf. Therefore the mass ratio, $q = M_{\mathrm{dMe}}/M_{\mathrm{DA}}$, is 0.76 ± 0.04. The separation of the binary is 1.32 ± 0.03 $R_{\odot}$, assuming a circular orbit. The radius of the Roche lobe for this system is 0.47 ± 0.01 $R_{\odot}$, which is only slightly larger than the radius of the secondary measured from the width of the Hα emission in § 3.1.2. Therefore the red dwarf is close to filling its Roche lobe.

The light curves also show ellipsoidal variations from the distorted red dwarf companion. The amplitude of the varia-

tions are 0.194 and 0.050 in *R* and *B*, respectively. The true amplitude of the ellipsoidal variation corrected for white dwarf continuum dilution estimated from the eclipse is $\Delta R = 0.24 \pm 0.02$ and $\Delta B = 0.21 \pm 0.09$. This amplitude can be used to determine the inclination of the system, but it is also sensitive to the value used for gravitational darkening (Warner 1995). Adopting $i = 73°5$ and using the gravitational darkening coefficient at 7000 Å, $u_g = 1.29$ (Russell 1945; Kopal 1959), we predict an amplitude of 0.275 ± 0.013, compared with 0.170 ± 0.008 for $u_g = 0.412$ (Lucy 1967) and 0.151 ± 0.007 for $u_g = 0.257$ (Claret 2000), where we have assumed a blackbody spectrum of the red dwarf. This last assumption is probably responsible for a mismatch between predicted and observed amplitudes, and detailed light-curve modeling might prove successful in constraining the inclination and mass ratio independently.

4. SUMMARY

We have updated the ephemerides of the close binaries EUVE J0720−31.7 and BPM 6502, and measured new orbital parameters for the binaries BPM 71214 (Table 7) and EC 13471−1258 (Table 8). The new ephemeris for EUVE J0720−31.7 will be used in later work to combine phase-resolved spectroscopy obtained with the *HST* GHRS in 1996 September and October, and with *FUSE* in 2001 November. The red dwarf in BPM 6502 clearly shows the effect of reprocessing of incoming radiation from the white dwarf in both Hα emission strength and *I/R* photometry. New orbital periods of BPM 71214 and EC 13471−1258 have been measured, with EC 13471−1258 being an eclipsing binary. The absence of an accretion disk but with a filled Roche lobe suggests that EC 13471−1258 is a hibernating nova (Shara
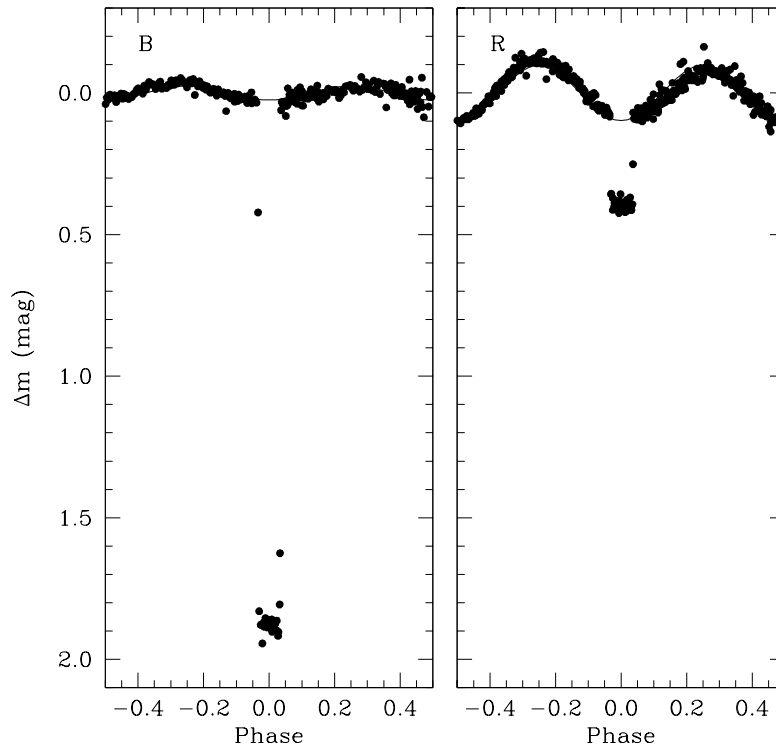

Fig. 13.—Photometry of EC 13471−1258 in *R* and *B* showing the ellipsoidal variations and the eclipse. The depth of the eclipse is 0.3 mag in *R* and 1.85 mag in *B* with a duration of 15.4 minutes, and the semiamplitudes of the ellipsoidal variations are 0.097 and 0.025 mag in *R* and *B*, respectively. There is no evidence of illumination of the red dwarf by the white dwarf.

TABLE 7
PROPERTIES OF THE BINARY BPM 71214

Parameter	Measurement	Reference
R.A. (epoch = 1997.745)	3 32 43.44 (J2000.0)	1
Decl. (epoch = 1997.745).......	−8 55 39.6 (J2000.0)	1
V, R	13.49, 12.81	2
B....................................	14.2	3
Spectral type	DA + M2.5 V	4
WD effective temperature.......................	$T_{eff} = 17200 \pm 1000$ K	4
WD surface gravity	$\log g = 8.25 \pm 0.10$	4
Binary orbital period..............	$P = 0.20162 \pm 0.00004$ days	4
Red dwarf semiamplitude....................	$K_{dMe} = 123.6 \pm 2.1$ km s^{-1}	4
Systemic velocity....................	46.2 ± 1.5 km s^{-1}	4
Mass function	$0.039 \pm 0.002\ M_\odot$	4
Mass of WD..........................	$0.77 \pm 0.06\ M_\odot$	4
Mass of RD...........................	$0.40\ M_\odot$ (estimated)	4
Orbital separation	$1.5\ R_\odot$ (estimated)	4
Inclination	30° (estimated)	4
Proper motion.......................	$\mu = 0.143$ mas	3
	$\pi = 137°$	3

REFERENCES.—(1) Digitized Sky Survey; (2) GSC II; (3) Luyten 1963 ; (4) this work.

TABLE 8
PROPERTIES OF THE BINARY EC 13471−1258

Parameter	Measurement	Reference
R.A. (epoch = 1985.167)	13 49 51.95 (J2000.0)	1
Decl. (epoch = 1985.167).......	−13 13 37.5 (J2000.0)	1
V...	14.7	2
Spectral type	DA + M2–4	3
WD effective temperature.......................	$T_{eff} = 14085 \pm 100$ K	3
WD surface gravity	$\log g = 8.25 \pm 0.05$	3
Binary orbital period..............	$P = 0.15074 \pm 0.00004$ days	3
Red dwarf semiamplitude....................	241.0 ± 8.1 km s^{-1}	3
Systemic velocity....................	-28.1 ± 5.9 km s^{-1}	3
Mass function	$0.219 \pm 0.022\ M_\odot$	3
Mass of WD..........................	$0.77 \pm 0.04\ M_\odot$	3
Mass of RD...........................	$0.58 \pm 0.05\ M_\odot$	3
Orbital separation	$1.32 \pm 0.03\ R_\odot$	3
Inclination	$73°5 \pm 1°1$	3

REFERENCES.—(1) Digitized Sky Survey; (2) Kilkenny et al. 1997; (3) this work.

et al. 1986). The system BPM 71214 closely resembles EC 13471−1258 but at a much lower inclination. The red dwarf stars in BPM 71214 EC 13471−1258 are extremely active and may contribute to a study of the effect of rotation on coronal activity.

REFERENCES

Allard, N. F., & Koester, D. 1992, A&A, 258, 464
Christian, D. J., & Mathioudakis, M. 2002, AJ, 123, 2796
Claret, A. 2000, A&A, 359, 289
Dupuis, J., Vennes, S., & Bowyer, S. 1997, in White Dwarfs, ed. I. Isern et al. (Dordrecht: Kluwer), 277
Hillwig, T. C., Honeycutt, R. K., & Robertson, J. W. 2000, AJ, 120, 1113
Houdebine, E. R., & Doyle, J. G. 1994, A&A, 289, 169
Hubeny, I., & Lanz, T. 1995, ApJ, 439, 875
James, D. J., Jardine, M. M., Jeffries, R. D., Randich, S., Cameron, A. C., & Ferreira, M. 2000, MNRAS, 318, 1217
Kawka, A., Vennes, S., Dupuis, J., & Koch, R. 2000, AJ, 120, 3250 (K2000)
Kilkenny, D., O'Donoghue, D., Koen, C., Stobie, R. S., & Chen, A. 1997, MNRAS, 287, 867
Kopal, Z. 1959, Close Binary Systems (London: Chapman & Hall)
Livio, M., & Shara, M. M. 1987, ApJ, 319, 819
Lucy, L. B. 1967, Z. Astrophys., 65, 89
Luyten, W. J. 1963, Bruce Proper Motion Survey, The General Catalogue (Minneapolis: Univ. Minnesota Press)
Marsh, T. R. 2000, NewA Rev., 44, 119
Mihalas, D., Auer, L. H., & Heasley, J. N. 1975, A Non-LTE Model Stellar Atmosphere Computer Program (NCAR-TN-STR+104)

O'Brien, M. S., Bond, H. E., & Sion, E. M. 2001, ApJ, 563, 971
Orosz, J. A., Wade, R. A., Harlow, J. J. B., Thorstensen, J. R., Taylor, C. J., & Eracleous, M. 1999, AJ, 117, 1598
Pickles, A. J. 1998, PASP, 110, 863
Russell, N. R. 1945, ApJ, 102, 1
Schechter, P. L., Mateo, M., & Saha, A. 1993, PASP, 105, 1342
Schmidt, G. D., Smith, P. S., Harvey, D. A., & Grauer, A. D. 1995, AJ, 110, 398
Shara, M. M., Livio, M., Moffat, A. F. J., & Orio, M. 1986, ApJ, 311, 163
Somers, M. W., Lockley, J. J., Naylor, T., & Wood, J. H. 1996, MNRAS, 280, 1277
Thorstensen, J. R., Charles, P. A., Margon, B., & Bowyer, S. 1978, ApJ, 223, 260
Vennes, S. 1999, ApJ, 525, 995
Vennes, S., & Thorstensen, J. R. 1994, ApJ, 433, L29
———. 1996, AJ, 112, 284
Voges, W., et al. 1999, A&A, 349, 389
Warner, B. 1995, Cataclysmic Variable Stars (Cambridge: Cambridge Univ. Press), 119
Wood, M. A. 1995, in White Dwarfs, ed. D. Koester & K. Werner (New York: Springer), 41